KU LEUVEN

STADIUS
Center for Dynamical Systems, Signal Processing and Data Analytics

Citation/Reference	Bernardi G., van Waterschoot T., Moonen M., Wouters J., Hillbratt M., and Verhaert N., **Measurement and Analysis of Feedback and Nonlinearities for the Codacs™ Direct Acoustic Cochlear Implant** *IEEE Access*, vol. 5, no. 1, Dec. 2017, pp. 8702-8713.
Archived version	Author manuscript: the content is identical to the content of the published paper, including the final typesetting by the publisher
Published version	http://ieeexplore.ieee.org/document/7926368/
Journal homepage	http://ieeexplore.ieee.org/xpl/RecentIssue.jsp?punumber=6287639
Author contact	giuliano.bernardi@esat.kuleuven.be *+ 32 (0)16 321797*
IR	Klik hier als u tekst wilt invoeren.

(article begins on next page)

IEEE Access
Multidisciplinary | Rapid Review | Open Access Journal

Received February 20, 2017, accepted May 6, 2017, date of publication May 11, 2017, date of current version June 28, 2017.

Digital Object Identifier 10.1109/ACCESS.2017.2703635

Measurement and Analysis of Feedback and Nonlinearities for the Codacs Direct Acoustic Cochlear Implant

GIULIANO BERNARDI[1], (Student Member, IEEE), TOON VAN WATERSCHOOT[1,2], (Member, IEEE), MARC MOONEN[1,2], (Fellow, IEEE), JAN WOUTERS[3], MARTIN HILLBRATT[4], AND NICOLAS VERHAERT[3,5]

[1]Department of Electrical Engineering, ESAT-STADIUS, Katholieke Universiteit Leuven, B-3001 Leuven, Belgium
[2]AdvISe Lab, Department of Electrical Engineering, ESAT-ETC, B-2440 Geel, Belgium
[3]Lab ExpORL, Department of Neurosciences, Katholieke Universiteit Leuven, B-3000 Leuven, Belgium
[4]Mölnlycke Health Care, 487 Lindome, Sweden
[5]Department of Otolaryngology, Head and Neck Surgery, University Hospitals Leuven, B-3000 Leuven, Belgium

Corresponding author: Giuliano Bernardi (giuliano.bernardi@esat.kuleuven.be)

This work was supported in part by the ESAT Laboratory, in part by the ExpORL Laboratory of KU Leuven through the IWT O&O Project, Signal Processing and Automatic Fitting for Next Generation Cochlear Implants under Grant 110722, in part by the KU Leuven Research Council CoE under Grant PFV/10/002, in part by the Interuniversity Attractive Poles Programme initiated by the Belgian Science Policy Office, Dynamical Systems Control and Optimization 2012-2017 under Grant IUAP P7/19. The scientific responsibility is assumed by its authors.

ABSTRACT Acoustic feedback is a very common problem in hearing instruments. Not only does it occur in common behind-the-ear or in-the-ear hearing aids, it also affects bone conduction implants, middle ear implants, and more recent devices, such as the direct acoustic cochlear implant (DACI). In this paper, we present the data and analysis relating to the feedback path characterization of the Cochlear^{TM} Codacs^{TM} DACI, performed on fresh frozen cadaver heads in four different measurement sessions. The general objectives were the following: 1) To measure and analyze the feedback path of the system and check for possible specimen-dependent variabilities; 2) To assess whether this feedback path is affected by an incorrect implantation; 3) To check for nonlinear behavior; and 4) To determine differences between tissular and airborne feedback. The data analysis reveals that the feedback seems to be dependent on the specific head morphology of the implanted specimen, and that an incorrect implantation might strongly affect the feedback path; additionally, the analysis reveals that some nonlinear behavior at high stimulus levels can be expected and, finally, that the feedback path is characterized by a tissular feedback component with a rather different frequency content compared to the airborne feedback component.

INDEX TERMS Hearing aids, direct acoustic cochlear implant (DACI), acoustic feedback, impulse response measurements, nonlinearities.

I. INTRODUCTION

Hearing loss occurs when some form of impairment affects the auditory system. Given the complex structure of the auditory system, a broad spectrum of problems can affect normal hearing. For this reason, in the last five decades, several types of hearing instruments have been designed to cope with these different hearing loss conditions. Various solutions have been specifically designed for both conductive hearing loss and sensorineural hearing loss, while mixed hearing loss, in particular when severe to profound, could not be addressed with a dedicated solution until the last decade. One of the implants able to cope with such a problem is the so-called direct acoustic cochlear implant (DACI) [1], see fig. 1.

The Cochlear^{TM} Codacs^{TM} DACI consists of an implantable electro-mechanical actuator, placed within the mastoid cavity and firmly fixed through a bone plate, see fig. 1b and fig. 1c, directly stimulating the cochlea via a piston prosthesis coupled to an artificial actuator [2]. The implanted actuator is controlled and driven from the outside through an RF link, and can be interfaced with the standard Cochlear behind-the-ear (BTE) sound processor (originally developed for cochlear implants). The Codacs DACI has been proven

2169-3536 © 2017 IEEE. Translations and content mining are permitted for academic research only.
Personal use is also permitted, but republication/redistribution requires IEEE permission.
See http://www.ieee.org/publications_standards/publications/rights/index.html for more information.

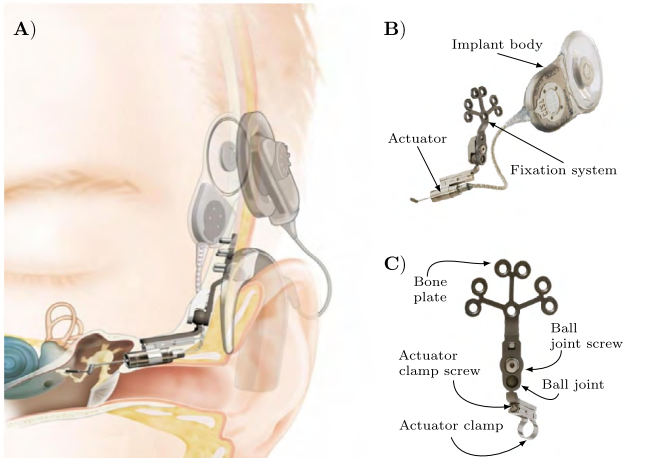

FIGURE 1. Details of the Cochlear™ Codacs™ DACI. A) Scheme showing both the implanted and the external parts of the device. B) Implantable parts. C) Fixation system. Courtesy of Cochlear Ltd.

to be effective in the treatment of severe-to-profound mixed hearing loss [3]; however, the follow-up monitoring of some patients that received the implant suggested that acoustic feedback can occur [4].

In order to tackle the feedback problem, some kind of feedback control is needed. A widely used strategy to control acoustic feedback involves the use of an adaptive feedback cancellation (AFC) algorithm, where a filter adaptively estimates the unknown feedback path and hence the unknown feedback signal, which is then subtracted from the microphone signal [5], [6]. The design of an AFC algorithm can be simplified if some prior knowledge of the feedback path is available. For instance, from single or multiple characterizations of the feedback path, one can evaluate the presence of nonlinearities, the time- and frequency-domain structure of the feedback path, as well as tune some critical parameters of the AFC algorithm, such as the filter length and the overall scaling factor of the filter coefficients [7], [8]. Additionally, the variability introduced by changes in the hearing aid (HA) working conditions, e. g. due to a hand or a different reflector nearby the HA microphone, can be evaluated [9], [10].

A characterization of the feedback path, either on test subjects or mannequin heads, using random noise signals is often performed in the literature introducing AFC and other feedback-control algorithms for HAs applications [7], [9], [11]–[13]. The characterization measurements presented in this paper, instead, were carried out on fresh frozen cadaver heads; this was done because the Codacs DACI is an implantable device, and hence cannot be mounted on a mannequin head, and because any risk for the implanted patients deriving from excessive stimulation needed to be avoided. Additionally, the characterization was performed using the exponential sine sweep (ESS) technique, allowing to monitor the nonlinear content of the system under test [14].

The measurements and analysis of the feedback path of the Codacs DACI presented in this paper had multiple general objectives. First, the feedback path of this novel hearing instrument was measured, providing information in terms of filter length, levels and spectral shape given that this knowledge can simplify the design of a feedback canceller. The tests were performed on four cadaver heads to verify possible feedback variabilities. Second, the measurements were performed in a case of an incorrect actuator positioning (i. e. the actuator touched the bone of the posterior wall of the external ear canal) to assess whether this could lead to an increase of the feedback energy in possibly critical regions. Third, the presence of nonlinearities was investigated, since these can have a profound impact on the performance of standard feedback cancellers. Finally, it was assessed whether the feedback path impulse response (IR) measured with the microphone positioned on a standard BTE sound processor differs from the IR measured with an external (and mechanically decoupled) microphone. This is done to verify whether the mechanical coupling between the DACI and the BTE microphone, through the bone tissue and the soft tissue layers, gives rise to a significant non-airborne, referred to as tissular, feedback component. The term mechanical coupling is used loosely to indicate the mechanical interactions between the DACI and the BTE microphone, caused mainly by the fixation of the DACI to the temporal bone and, to a lesser extent, by the connection between the DACI and the cochlea. Thus, by tissular feedback we mean the acoustic feedback propagating mainly through bone and soft tissue layers and not through air.

II. MATERIALS AND METHODS

A. CODACS ACTUATOR TRANSFER FUNCTION

The Codacs DACI is characterized by a strong resonance in the actuator transfer function (ATF) [15]. The ATF is the transfer function measured on the bench between an applied voltage and the induced stapes prosthesis velocity and it is expressed in m/s/V [16]. Laser-Doppler-vibrometry measurements show that the ATF exhibits a resonance around 2 kHz, that can slightly shift when using different actuators. In implanted patients, a more relevant source of variability is due to implantation and postoperative processes such as healing and scarring. The impact of these phenomena is discussed later in section IV-A. The effect of the resonance is usually precompensated by filtering the signal fed to the actuator with the inverse ATF.

Two Codacs actuators, referred to as `act1` and `act2`, were used in the different measurement sessions (MSs) (`act1` in MS1, MS2 and MS3, `act2` in MS4); their frequency responses are shown in fig. 2.

B. FEEDBACK SYSTEM DESCRIPTION

Figure 3 depicts the simplified block diagram of an implanted Codacs DACI, operating in a closed-loop scenario. This does not represent the tested system described in this paper, but it is helpful to contextualize how a characterization of the feedback path of the implanted device can be helpful to the design of an AFC algorithm. Each block in the scheme is

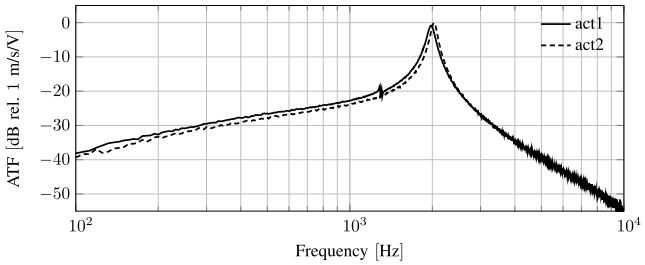

FIGURE 2. Vibration velocity to voltage sensitivity as a function of frequency for the two Codacs actuators (`act1` and `act2`) used throughout the four MSs.

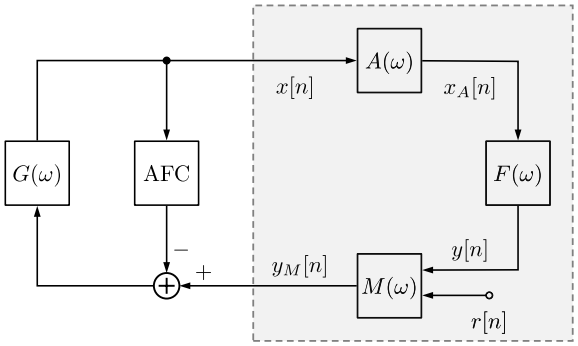

FIGURE 3. Simplified block diagram of an implanted Codacs DACI operating in closed-loop , where $M(\omega)$, $A(\omega)$, $G(\omega)$ and $F(\omega)$ represents the frequency responses of the BTE microphone, the Codacs actuator, the sound processor, and the feedback path, respectively, AFC represents the AFC algorithm, and $r[n]$ represents the source signal (such as speech or background noise). The shaded portion of the diagram refers to the open-loop system, schematizing the measurement scenario of the different MSs.

represented via its frequency response, defined as a function of the angular frequency ω. The rightmost block $F(\omega)$ represents the feedback path frequency response, expressed in m/s/Pa, relating the actuator velocity to the pressure level recorded by the microphone. The Codacs DACI is schematically represented by three main parts: the BTE microphone characterized by $M(\omega)$, the Codacs actuator characterized by $A(\omega)$, and the sound processor characterized by $G(\omega)$.

At high stimulation levels, the actuator is assumed to be a weakly nonlinear system, as often done for loudspeakers, and can be modeled by means of memoryless Volterra series [14], [17]. In a hearing aid scenario $G(\omega)$ is often including some kind of nonlinear processing (e. g. compression), too. The frequency responses $M(\omega)$, and $F(\omega)$ are assumed to be linear and time-invariant, meaning that they can be all replaced by means of the correspondent IRs, i. e. $m[n]$ and $f[n]$. In such a case, the microphone signal $y_M[n]$ is obtained from the addition of two signals: $r[n]$ is the source signal given by the desired component to process and amplify, such as speech or music, and possibly some background noise; $y[n]$ is the feedback signal, obtained by filtering the stimulus $x_A[n]$ generated by the Codacs actuator through the feedback path IR $f[n]$, i. e. $y[n] = f[n] * x_A[n]$ where $*$ denotes convolution, contributing to the closure of the feedback loop. Memoryless Volterra series provide a compact way to describe the relation between $x[n]$ and $x_A[n]$ by means of the Volterra kernels, i. e. $a_k[n]$ with $k = 1, \ldots, K$; however, discussing such a relation is outside the scope of this paper. The cascaded feedback path IR can be included in the actuator's model by replacing the Volterra kernels $a_k[n]$ with the modified Volterra kernels of the system including both actuator and feedback path, i. e. $h_k[n]$ with $k = 1, \ldots, K$, whose estimates will be used later to define the nonlinearity measure. Specifically, the relation $h_1[n] = a_1[n] * f[n]$ holds [18]; under the assumption that the linear Volterra kernel $a_1[n]$ can be approximated by the ATF, a precompensation can be introduced by filtering the input signal $x[n]$ fed to the actuator with an estimate of the inverse $a_1[n]$, i. e. $\hat{a}_1^{-1}[n]$, to obtain the proportionality relation $h_1[n] \propto f[n]$ and hence simplify the identification procedure of $f[n]$.

If the nonlinearity assumption of the actuator is relaxed (this is reasonable at low stimulation levels, as will be shown in section III-C), and the same is done with $G(\omega)$, leading to a linear representation of $A(\omega)$ and $G(\omega)$, the stability of the closed-loop system in fig. 3, in absence of the AFC block, can be analyzed [5], [6], [12]. Although assuming linearity for $G(\omega)$ is arguably simplistic in a hearing aid scenario, this is common in literature to keep the theoretical analysis treatable [7], [9], [19], [20]. The product between $F(\omega)$ and the forward path response, represented by $A(\omega)G(\omega)M(\omega)$, results in the so-called open-loop response $F(\omega)A(\omega)G(\omega)M(\omega)$. The analysis of the open-loop response is important since it allows to determine the stability of the closed-loop response from the source signal $r[n]$ to the actuator output signal $x_A[n]$, by means of their frequency responses $R(\omega)$ and $X_A(\omega)$, respectively:

$$\frac{X_A(\omega)}{R(\omega)} = \frac{A(\omega)G(\omega)M(\omega)}{1 - A(\omega)G(\omega)M(\omega)F(\omega)}. \tag{1}$$

Therefore, the estimation of $F(\omega)$ discussed in this paper represents an important first step to calculate the open-loop response of the system under test that will be used in the stability analysis and control.

C. FEEDBACK PATH ESTIMATION

In measurements performed for this study, we used the ESS technique [14], widely used in room impulse response (RIR) measurements [18], [21]. The ESS technique is used to estimate the feedback path IR $f[n]$ and to investigate the nonlinear behavior of the actuator.

A mathematical description of the ESS stimulus is given by

$$x_{\mathrm{ESS}}[n] = \sin\left\{\frac{\omega_1 T}{\ln(\omega_2/\omega_1)}\left[\left(\frac{\omega_2}{\omega_1}\right)^{\frac{n}{T}} - 1\right]\right\}, \tag{2}$$

where ω_1 and ω_2 are the starting and ending angular frequencies of the sweep, and T is the duration of the sweep in s. Hence, the ESS stimulus has a frequency content that exponentially varies with time with a roughly pink spectrum (i. e. -3 dB/Octave). Usually, a fade-in and fade-out stage at the extremes of the sweep is also included [21]. In the current study, we used a 2000-samples Hann window.

Referring to fig. 3, the input and output of our measurements were $x[n]$ and $y_M[n]$, respectively. The actuator was fed with a precompensated stimulus $x[n]$, obtained by filtering $x_{\mathrm{ESS}}[n]$ via the inverse of the available ATFs, i. e. $x[n] = x_{\mathrm{ESS}}[n] * \hat{a}_1^{-1}[n]$. This was mainly done in order to prevent overstimulation and extreme distortion that might be induced by the actuator's resonance, but also to simplify the identification procedure, as seen in section II-B. By doing so, a first order approximation of the input fed to the feedback path $F(\omega)$ is $x[n] * a_1[n] \approx x_{\mathrm{ESS}}[n]$.

The deconvolution procedure to estimate $f[n]$ is easily obtained by filtering the measured output signal $y_M[n]$ with the time-reversed version of $x_{\mathrm{ESS}}[n]$ [14]. The ESS deconvolution results in a signal, from now on referred to as deconvolved total response (DTR), characterized by a sequence of time-separated responses, cf. fig. 4, each representing a different-order harmonic distortion. If the system is linear and the linear Volterra kernel $a_1[n]$ is properly compensated for, the sequence consists of a single response proportional to an estimate of the feedback path IR $f[n]$, i. e. $\hat{h}_1[n]$, from now on referred to as deconvolved impulse response (DIR). In case of a nonlinear system, other higher-order harmonics, i. e. $\hat{h}_k[n]$ for $k = 2, \ldots, K$, will appear before the DIR [14]. The DTR can be compactly defined as $\hat{h}[n] = \sum_{k=1}^{K} \hat{h}_k[n]$.

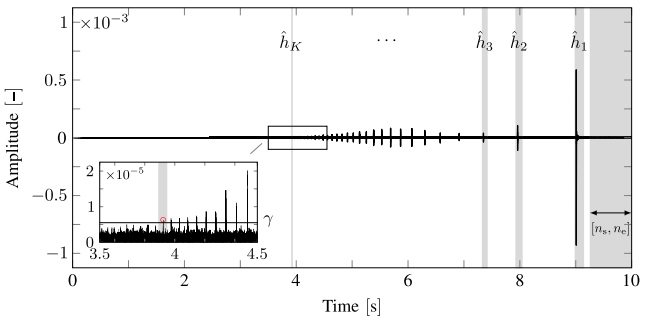

FIGURE 4. Example of a DTR in the time domain from one of the measured BTE microphone signals. The inset shows the amplitude absolute values in the part of the response surrounding the Kth harmonic, with ranges 3.5 s to 4.5 s and 0 to 2.5×10^{-5} in the x- and y-axis respectively, and helps to compare the amplitudes of the harmonics and those of the noise floor (i. e. $n \in [n_s, n_e]$).

In reality, the measured output signal $y_M[n]$ includes the effect of the microphone transfer function, too, when the latter is not flat. More details will be given in section IV.

A sampling frequency $f_s = 44.1$ kHz was employed during the measurements and the stimuli were constructed as follows: The length of the ESS was set to be 8 s and the swept was between 50 and 10 000 Hz. Two seconds of silence were placed between each of the five sweeps repeated for each of the four applied ESS stimulus levels, i. e. 0.18, 0.35, 0.53, and 0.71 $\mathrm{V_{RMS}}$. The highest tested level was chosen considering that the actuator's internal magnetic circuit starts saturating above 0.71 $\mathrm{V_{RMS}}$, and corresponds to an equivalent sound pressure level between 120 and 130 dB SPLeq; the other levels were chosen to be linearly spaced between 0 and 0.71 $\mathrm{V_{RMS}}$. In a patient, the stimulus levels are usually in lower than 10 $\mathrm{mV_{RMS}}$ [22], but they can easily reach levels in the order of hundreds of $\mathrm{mV_{RMS}}$ (private communication with the manufacturer). The stimulus levels used in this study were chosen to be higher in order to cope with the low signal-to-noise ratio (SNR) of the measurement room.

The choice of retaining only five repetitions of the sweep per measurement was mainly driven by practical constrains, such as the non-ideal acoustic conditions of the room (e. g. the presence of impulsive noise) and the limited time that could be allocated to the use of each cadaver head during the measurements. Due to the difficulties of recording five consecutive sweeps without any impulsive background noise corruption, several recordings were taken and only those with the lowest (or absent) traces of impulsive noise were retained and patched together for the subsequent analysis. Assuming additive and uncorrelated background noise, the coherent averaging of the five recorded sweep responses allowed to reduce the noise floor by approximately $10 \log_{10}(5) \approx 7$ dB.

D. DISTORTION MEASURE

A common nonlinear distortion measure employed to characterize (acoustic) nonlinear systems is the so-called total harmonic distortion (THD) [23]. Unfortunately, an extension of the THD to be used with the ESS technique has not been developed yet. Additionally, in our measurements, it was not feasible to carry out an extensive THD characterization measurement, consisting of single tone stimulations repeated at each tested frequency, due to the time constraint imposed by the use of cadaver heads. Therefore, we introduce a nonlinear distortion measure calculated using only easily distinguishable features from the DTRs.

Figure 4 provides an example of a DTR from one of our recordings, highlighting some of the key parameters for the calculation of the proposed nonlinear distortion measure, where the gray shaded areas $\hat{h}_k[n]$ are estimates of the modified Volterra kernels $h_k[n]$. The shaded area $\hat{h}_1[n]$ in the righthand side of the figure approximates the linear modified Volterra kernel, shown to be proportional to $f[n]$, while the other shaded areas $\hat{h}_2[n] \ldots \hat{h}_K[n]$ approximate the higher order kernels, related to the 2nd to K^{th} harmonics [14]. K was chosen to be the minimum number of identifiable maxima in the DTR, after a lower threshold value for the maxima was fixed, i. e. no maximum below the threshold was retained. This was done in order to avoid selecting spurious noise peaks with amplitude comparable to the true higher order harmonics. The threshold was estimated from the rightmost portion of $\hat{h}[n]$ in fig. 4, i. e. for $n \in [n_s, n_e]$, assumed to contain only noise. Such an assumption should be fulfilled, given that n_s was chosen 0.2 s after the beginning of the linear part $\hat{h}_1[n]$ and, as we will see in section III, 0.2 s is approximately one order of magnitude greater than the decay time of the $\hat{h}_1[n]$. Specifically, the threshold was conservatively calculated as $\gamma = \max_{n \in [n_s, n_e]} \left\{ |\hat{h}[n]| \right\}$. The inset of fig. 4 helps to visually compare the amplitude absolute values of the different harmonics and those of the noise floor samples. The circled relative maximum represents the value

of $\max\left\{|\hat{h}_K[n]|\right\}$, i. e. the lowest supra-threshold value, in the specific situation.

The calculation of THD requires an estimation of the power of each harmonic. However, this is not easily done with our measurements due to the low SNR. Therefore, our distortion measure D is calculated using only the amplitude absolute value maxima of the different harmonics:

$$D = \frac{\sum_{k=2}^{K}\left[\max\left\{|\hat{h}_k[n]|\right\}\right]^2}{\left[\max\left\{|\hat{h}_1[n]|\right\}\right]^2}. \quad (3)$$

It must be pointed out that this nonlinear distortion measure does not necessarily provide a general indicator of system nonlinearity, comparable to other known measures like THD, but it provides a means to compare the results collected in our measurements from different sessions, using different excitation levels and different implantation schemes.

E. CADAVER HEADS MEASUREMENTS

All the feedback path measurements on thawed fresh frozen cadaver heads took place in the ENT Department (Saint-Luc University Hospital, Brussels, Belgium) between July 2013 and June 2014 for a total of four MSs and the study was approved by the local ethical committee. Entire heads were evaluated after obtaining authorization to use organs and tissues for research (Science Care, Inc., Phoenix, AZ, USA). The medical history of each head was provided by the supplying company to exclude any otologic pathology. In each of the MSs, a different cadaver head was used and the surgery was performed on the right ear, after any residual earwax had been removed and otomicroscopy verified an intact ear drum and the absence of ear pathology. Surgical preparation was carried out similarly for all four MSs and included a routine Codacs implantation [4]. In detail, it consisted of a canal wall-up mastoidectomy with preservation of the posterior border of the mastoid cavity for placement of the implant's fixation system. A large posterior tympanotomy was performed by opening the facial recess. Care was taken not to touch the ossicular chain avoiding trauma to the ossicles and eardrum. Subsequently, exposure of stapes crurae and stapes footplate was obtained. After a stapedotomy, allowing to verify that the cochlea was filled with fluid, and fixation of the actuator in the mastoid cavity, a stapes prosthesis was coupled to an actuator. The stapedotomy opening was subsequently sealed with fibrous tissue. No additional middle-ear transfer functions were obtained as with the Codacs surgery the ossicular chain is interrupted. Finally, in order to reproduce real-life implantation, the wound was closed with sutures in a double-layer technique. A small actuator lead was passed through the incision between two sutures to avoid leakage.

The choice of using cadaver heads was made in order to be able to perform the measurements at high stimulation levels, possibly uncomfortable for implanted patients, such that a higher SNR could be achieved. Furthermore, in this way, an incorrect implantation, thought to be a possible cause of the problems highlighted in some of the follow-up cases in living patients, could be tested. The measurements were carried out in a room that was not acoustically treated, due to the practical difficulties of moving the cadaver heads to a separate acoustically shielded measurement room.

The stimuli were digitally created using a laptop, transmitted to a soundcard (RME Fireface UCX) and passed through a laboratory power amplifier (N4L LPA01) which was directly connected to the Codacs actuator. This measurement setup corresponds to direct stimulation in the sense that the sound processor was bypassed. The output signal of the amplifier was also sent back to the soundcard as a control signal to assess that this initial part of the signal path was not introducing any nonlinear distortion. Simultaneously to playing back the stimuli, the acoustic signal at the output of the ear canal were recorded by means of three microphones: a microphone embodied in the BTE case mounted on the cadaver head which, from now on, will be referred to as BTE microphone; a Brüel & Kjær 4190-L-001 with a 2690-A NEXUS microphone conditioner and an AKG CK 97-C, from now on referred to as airborne1 (AB1) and airborne2 (AB2) microphone, respectively. These two external microphones were hung at a distance of roughly 3-to-5 cm from the ear of the cadaver and placed so as to avoid any contact between each other. All the processing stages of the BTE sound processor were bypassed, except for the 12-ms input/output delay. The three microphones were connected to the soundcard, their recordings were digitized, using a 24-bit precision, and transferred back to the laptop in real time. The choice of using two airborne (AB) microphones was done to increase the MS setup redundancy. However, due to the unforseen unreliability of the AB2, exhibiting a level-dependent behavior at low frequency for the tested levels, we focused on the AB1 microphone solely. Real pictures of the setup are shown in fig. 5A-C.

Two of the four MSs returned only partial data: In MS3 the AB1 microphone was not available, while in MS4 we did not perform the full set of measurements carried out in the other three sessions, but only tested the highest stimulus level. Nevertheless, in MS4 we were able to test the differences originating from a correct implantation and a specific type of incorrect implantation of the device. In this paper, incorrect implantation refers to the case in which the tip of the Codacs actuator touched the bone of the posterior wall of the external ear canal. Other types of incorrect implantation could occur but we did not consider them in this work.

F. CALIBRATION MEASUREMENT

In addition to the cadaver heads measurements, we performed a microphone calibration measurement, in order to map the recorded levels from the BTE and the AB1 microphones into dB SPL units. We only performed an amplitude calibration, i. e. no phase calibration was performed. The BTE microphone calibration was done using a small anechoic

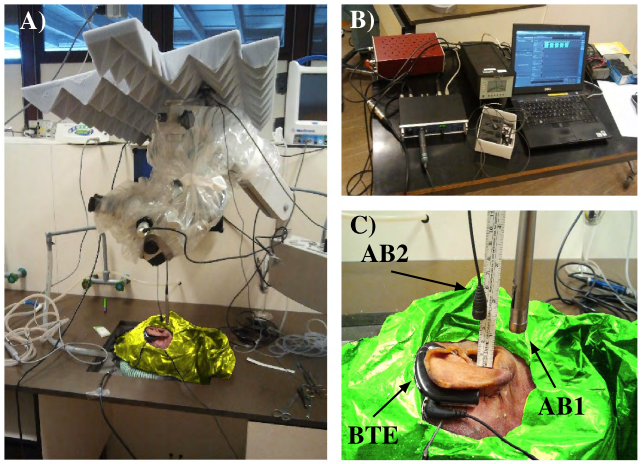

FIGURE 5. MSs setup. A) The cadaver head (right ear) with the implant in place and the three microphones ready to record. B) The instrumentation used for the measurements. C) A close-up of the cadaver head (right ear). In both A) and C), the plastic bag around the head has been digitally colored to differentiate its original black color from the colors of the microphones.

chamber (Brüel & Kjær 4222) together with a Pressure-field 1/2'' Brüel & Kjær 4192 reference microphone, and the AB1 microphone calibration was done using a Brüel & Kjær 4230 sound level calibrator.

G. DATA PRESENTATION

The time-domain signals shown in this paper are either microphone signals, DTRs or DIRs. The microphone signals are expressed in V, while both the DTRs and the DIRs are adimensional, see section II-B. In the DIRs plots, we simply set the time origin of our plots in correspondence with the DIRs first peak. This was done due to the small distance between the actuator and the BTE/AB1 microphone (less than 10 cm), which would correspond to a direct-sound delay on the order of tenths of ms. Such a small delay would be negligible compared to the actual processing delay introduced by the sound processor in an implanted patient (at least two orders of magnitude smaller).

The frequency-domain signals shown in this paper are either magnitude responses or power spectral densitiess (PSDs): the magnitude response of the DIRs were calculated using only the linear part of the DTR, considered to be a deterministic signal; the PSDs were used to qualify the whole calibrated microphone signals, considered to be stochastic signals. Furthermore, when showing the BTE PSDs, the dB SPL levels were forced to $-\infty$ above 7 kHz, to avoid improper scaling due to the strong high-frequency cutoff of the BTE microphone.

III. RESULTS

A. CADAVER HEADS MEASUREMENTS

Figure 6 shows the raw microphone signals (together with their spectrograms) for both BTE and AB1 microphones when the system was excited with a 0.71 V_{RMS} ESS stimulus in MS4. We notice that the actuator behaves in a nonlinear

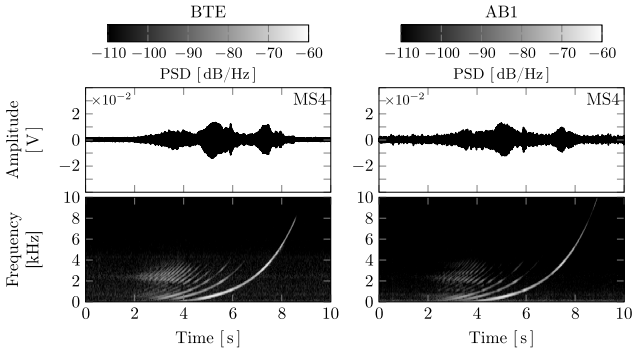

FIGURE 6. Recorded microphone signals and corresponding spectrograms from BTE and AB1 microphones obtained with a 0.71 V_{RMS} ESS stimulus in MS4.

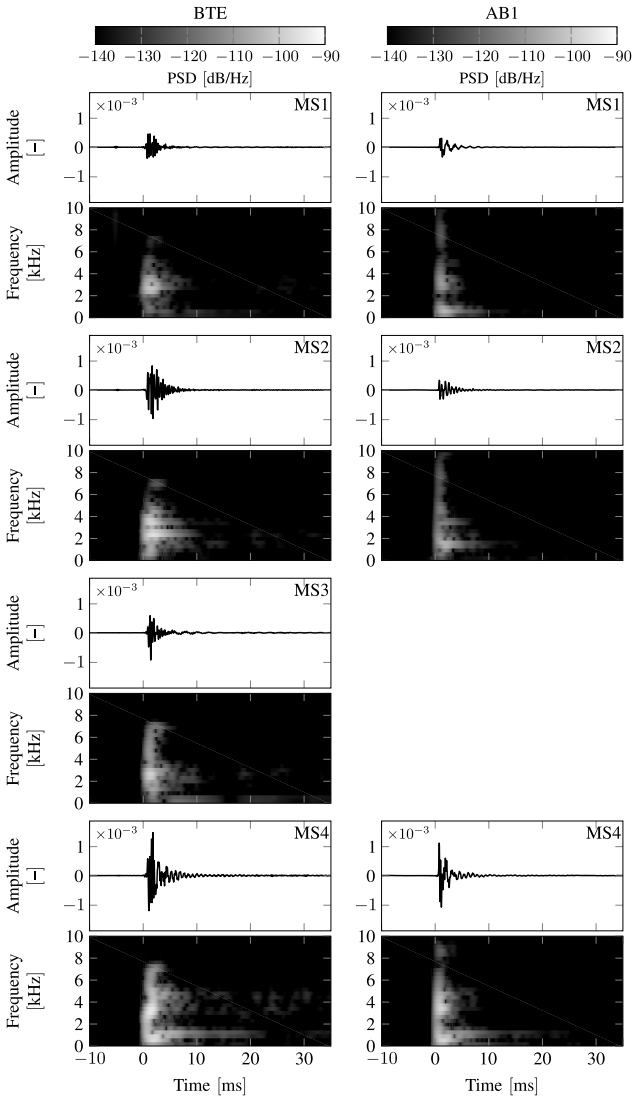

FIGURE 7. DIRs and corresponding spectrograms from BTE and AB1 microphone signals obtained with a 0.71 V_{RMS} ESS stimulus in MS1 to MS4.

way, when excited with the highest tested level, as indicated by the visible higher-order harmonics observed in both microphones signals (no copies of the original sweep should

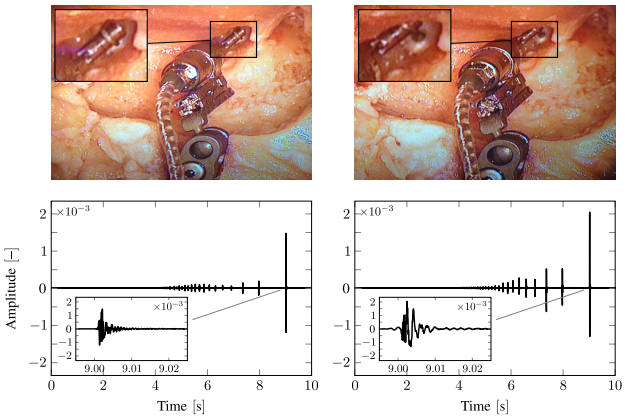

FIGURE 8. Top: Correct and incorrect placement of the Codacs actuator (top-left and top-right, respectively). The incorrectly implanted actuator touches the surrounding bone of the posterior wall of the external ear canal (compare the magnified area). Bottom: DTR from BTE microphone signal using a 0.71 V_{RMS} ESS stimulus from the corresponding surgical cases shown above; the insets show the detail of the DIR only. In each inset, the boundaries of the y-axis are kept the same as in the DTR plot, while only 30 ms of signal are shown on the x-axis.

be visible if the system were linear). The frequency region at approximately 2600 ± 400 Hz is excited at times when the stimulus frequency ranges roughly from 80 to 500 Hz. Therefore, the excited harmonics are of rather high order (at least 35 harmonics, on a visual analysis). For the sake of brevity, the microphone signals from the other MSs and the other levels are not shown. However, we would like to point out that the nonlinearity pattern varies but preserves the same core structure in all the different measurements.

Figure 7 shows the DIRs for both BTE and AB1 microphones when the system was excited with a 0.71 V_{RMS} ESS stimulus, for all four MSs. The AB1 microphone recordings from MS3 are missing in fig. 7 (as well as in figs. 9 to 11) due to the non-availability of the AB1 microphone in MS3 (cf. section II-E). The data in fig. 7 show a variation of both BTE and AB1 microphones throughout the MSs. Moreover, the small time scale allows to appreciate the variation in the decay time of the responses over different MSs. In some cases, e. g. MS3 and MS4, the DIRs exhibit a slower decay in some narrow frequency bands (at approximately 500 Hz and between 800 to 900 Hz, respectively) compared to the remaining part of the spectrum, giving rise to an oscillating behavior that can last up to 20 ms. This effect can be seen in the time-domain signals but it is more easily observed in the spectrograms.

In MS4, we also investigated the variation of the nonlinear response for the case of a correctly implanted actuator to that of an incorrectly implanted one, top-left and top-right of fig. 8, respectively. In the same figure, the DTR is shown for both cases, with the same scaling. It can be seen how a wrong position strongly increases the nonlinearity. The DIR shows, too, an increased energy content visible from both the increased maximum amplitude and from the slower decay time (the latter can be noticed in the insets of the plots).

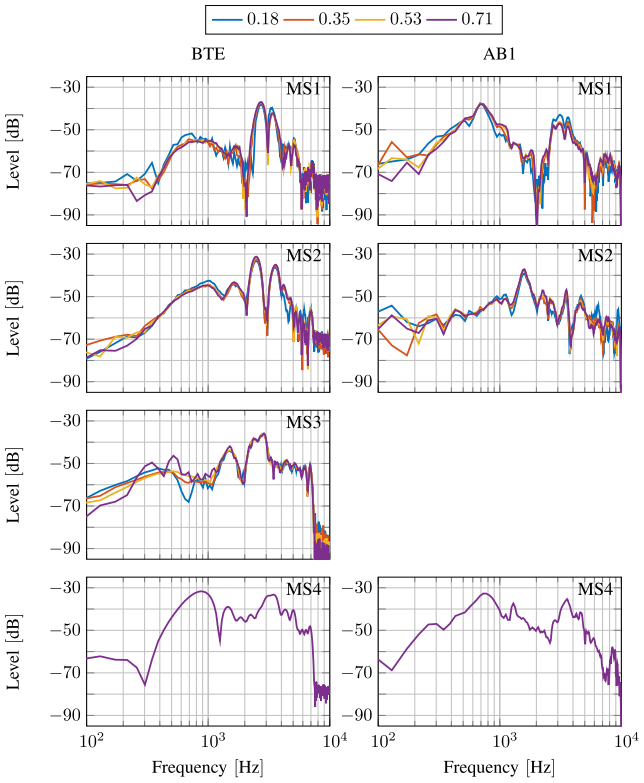

FIGURE 9. Magnitude response of the DIRs from BTE and AB1 microphone signals for the four tested levels in MS1 to MS4.

The magnitude responses of the DIRs from the BTE and AB1 microphone signals from MS1 to MS4 are shown in fig. 9. Each plot contains four magnitude responses, corresponding to the different ESS stimulus levels. The recordings of both BTE and AB1 microphones show variability among different MSs, e. g. the shift of the positions of peaks and dips and the change in the scaling. The magnitude response of the DIRs in a single session, for a single microphone, do not show a good degree of similarity in the whole spectrum. Specifically, a higher variability is shown in the low frequencies and in the frequency regions where the actuator behaves nonlinearly (80 to 500 Hz). The difference between the curves corresponding to the lowest and to the highest stimuli ranges between 4 to 14 dB for the BTE recordings and between 3 to 5 dB for the AB1 recordings.

B. APPLICATION OF THE MICROPHONES CALIBRATION MEASUREMENTS

Exploiting the data from the calibration of the microphones, cf. section II-F, allows to map the digital levels into dB SPL, hence simplifying the within-session comparisons by reducing the effect of each microphone transfer function from the magnitude responses. Unlike the results in fig. 9, in fig. 10 we can see that an increase in the stimulus level corresponds to an increase in the measured level. The effect is more easily noticeable in those frequency bands with energy well above the averaged background noise (from 5 repetitions, i. e. reduced by approximately 7 dB and defined bg_{-7} in the

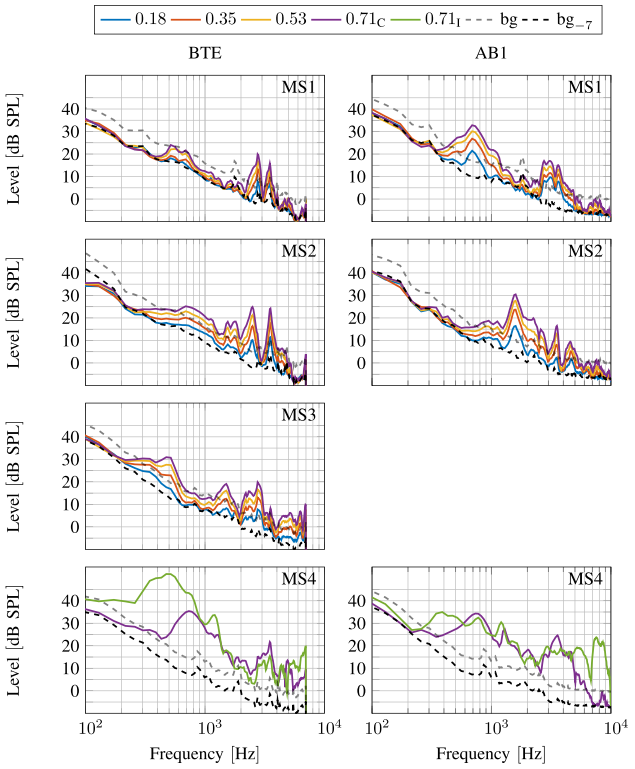

FIGURE 10. **Calibrated microphone PSDs in** dB SPL **of the BTE and AB1 microphones signals for the four tested levels, the background noise (bg) and the averaged background noise (bg_{-7}) in MS1 to MS4. The lower panels also include a comparison between the correctly implanted actuator (0.71_C) and the incorrectly implanted actuator (0.71_I) performed in MS4.**

figure), indicated by the black dashed line. Several differences can be seen throughout the different MSs and involve a frequency shift, as well as different magnitude, of peaks and dips in the PSDs, e. g. in MS2. By comparing the two microphone signals, mainly in MS1 and MS2, we can see that the peak centered around 700 Hz in MS1 and the peak at approximately 1500 Hz in MS2 show a roughly 10 dB stronger amplitude in the AB1 microphone PSD than the corresponding peak in the BTE microphone PSD. Other PSD components are shown to have a higher energy content in the BTE microphone signal: for instance, the two peaks at high frequency in MS1 and MS2 or the components between 200 to 1000 Hz in MS2. In MS4 there is a (visually) better correspondence, especially below 4000 Hz, between the components with highest energy in the BTE and AB1 microphone PSDs, still with some variability.

The lower panels of fig. 10 also shows the change in the microphone PSD levels going from the correctly implanted actuator to the incorrectly implanted actuator case. The resonance peak located at approximately 750 Hz in both microphone PSDs undergoes a frequency shift to approximately 500 Hz. However, the change in the magnitude of this component is very limited in the AB1 microphone PSD while it reaches up to 15 dB in the BTE microphone PSD. Other differences can be also observed, such as the increase in the

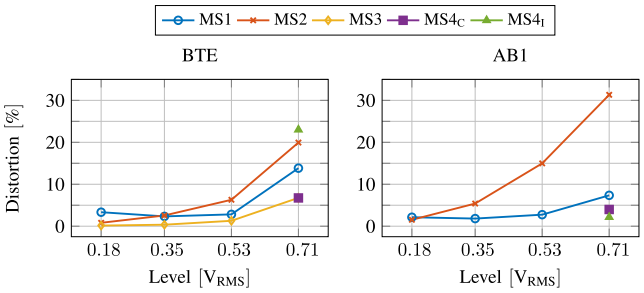

FIGURE 11. **Distortion calculated from BTE and AB1 microphone DTRs at different levels in MS1 to MS4 (the latter defined as $MS4_C$ in the legend), including the incorrectly implanted actuator results from MS4 ($MS4_I$).**

higher part of the spectrum for the AB1 microphone PSD, which is of little concern for the BTE microphone PSD due to its steep high-frequency cutoff.

C. NONLINEARITY OF THE SYSTEM

We conclude the section with the results of the *D* measure, cf. section II-D, presented in fig. 11. The values of *D* are estimated from the DTRs, i. e. where no microphone calibration is applied and, hence, only a same-microphone comparison is possible. The data show that an increase in the nonlinear response can be expected when increasing the stimulus level and that the nonlinear response is subject to variability between the different sessions. For the BTE microphone, the recordings in MS3 returns the lowest *D* values, while those in MS2 returns the greatest *D* values. A strong increase, slightly lower than 20 %, of the distortion measure from the correctly implanted actuator case to the incorrectly implanted actuator case for the BTE microphone can be observed in MS4. However, such an increase is not observed for the AB1 microphone, similarly to what is shown in the lower panels of fig. 10.

IV. DISCUSSION

A. ACTUATOR INPUT PRECOMPENSATION

An important issue to be mentioned about the measurements in this paper involves the concept of input precompensation, see section II-A. In particular, the difference between cadaver and patient input precompensation.

In implanted patients, a precompensation based on the intraoperatively-measured ATF is applied in the clinical software. However, in the postoperative phase, the intraoperatively-measured ATF resonance can be damped as well as slightly shifted by integration with the bony structures, and by soft tissue overgrowth due to healing and scarring, making the precompensation less effective. In the cadaver measurements we performed for this study, the precompensation was solely based on actuators ATF measured on the bench. Thus, the coupling and implantation can make, again, the precompensation less effective. Due to these limitations of the precompensation procedure, the design of a feedback canceller should be flexible enough to cope with both implantation and/or postoperative changes. Such

additional flexibility can be obtained by using, e. g., an AFC algorithm [19].

B. FEEDBACK PATH MEASUREMENTS

The results from section III suggest that the signals recorded with the same microphone in different MSs varies in both envelope and amplitude throughout the sessions. This can be seen both through the time variability of the signals in fig. 7 and through the frequency shift, as well as different magnitude, of peaks and dips from the magnitude responses in fig. 9. Due to the lack of microphone compensation in figs. 7 and 9, when visually comparing the content of different microphone signals (i. e. when performing an intermicrophone comparison), one should remember that the effects of the microphones' characteristics such as transfer function and microphone sensitivity are included in the microphone signals. Thus, the information in the figures depicting time-domain signals will be mainly used for the purpose of same-microphone comparison among MSs.

The within-session variability of the magnitude responses shown in fig. 9 can be accounted for by two main reasons: First, at low frequencies the SNR is the lowest, causing the estimation procedure to worsen. Second, the responses were calculated using only the linear part of the DTRs, meaning that the energy from the frequency components triggering the nonlinear behavior of the actuator has been removed. Nevertheless, a good correspondence of the magnitude responses can be seen at the resonant frequencies. This correspondence suggests that a similar behavior could be expected even at lower levels, matching more closely with the clinical range of operation. Had the experiments been conducted in a room with a higher SNR, we could reasonably expect an even lower within-session variability.

The intersession diversity seems to indicate that the changes in the specimen head morphology can cause variability in the feedback path response. This aspect should be recalled if the data from individual measurements were to be used in the fitting procedure of the Codacs DACI. In fact, the ESS technique could be used to estimate the specific feedback path magnitude responses of an implanted patient, returning a set of data similar to those in figs. 7 and 9 which represents useful information for the design of a frequency-domain feedback canceller, a common approach employed in hearing aids applications [9], [19]. These results could, in fact, be exploited as prior knowledge to tune the parameters of a feedback canceller during the fitting procedure, such as the filter length or the overall scaling factor of the filter coefficients, to provide faster convergence to the desired solution. Additionally, the maximum of each magnitude response from the BTE results in fig. 9 can be used, disregarding phase information, as an estimate of the feedback margin of the closed-loop system. This means that the feedback margin in the tested specimen, at the tested stimulus levels, and for the proposed simplifying assumptions [a flat, unit-magnitude transfer function for both $G(\omega)$ and $M(\omega)$, and a perfect compensation of $A(\omega)$] ranges between 29 to 37 dB. Since, in real applications, the assumptions made for the transfer functions $A(\omega)$ and $M(\omega)$ might not always hold, and the forward path gain $G(\omega)$ can easily reach values on the order of 60 dB in some frequency bands [24], the risk of triggering instabilities exists.

Similar considerations can be made for the oscillations in fig. 7: although the duration of these oscillations is very limited in time for our measurements, their effect could be worsened in a closed-loop scenario if these frequency bands were to contain, at a certain time, one or more unstable frequencies of the closed-loop system.

C. EFFECTS OF AN INCORRECT IMPLANTATION AND NONLINEAR BEHAVIOR

The data from the comparison between a correctly and incorrectly implanted actuator have suggested that an incorrect implantation could be detrimental in different ways when considering system feedback (cf. figs. 8, 10 and 11). The frequency shift and the increased energy content in the incorrectly implanted actuator case are caused by the drastic change in the acoustic loading of the system. The direct acoustic coupling between the actuator and the bone of the posterior wall of the external ear canal causes an increase in the acoustic impedance of the system, motivating the measured differences. This might indicate a possible correlation between incorrect implantation and induced acoustic feedback problems (a signal with greater energy would result in a greater feedback), possibly being the cause of the acoustic feedback described by [4]. Furthermore, the previously-mentioned detrimental effect of the oscillations in the DIR in combination with the longer decay time resulting from an incorrect implantation could lead, more likely than in the correctly implanted case, to instability in the closed-loop system. Finally, the presence of stronger nonlinearities compared to the correctly implanted actuator case (cf. fig. 11) is a further indication that complications could arise from incorrect implantation of the actuator, since an increase of the nonlinearity could cause a traditional (linear) feedback canceller to fail in its feedback path estimation procedure and, hence, ultimately fail in its feedback cancellation task.

As for the data discussed in the previous section, the data shown in the lower panels of fig. 10 only give a qualitative description of the possible differences arising from an incorrect implantation. From the single analyzed case, it would be unreasonable trying to extrapolate a threshold on the BTE-to-AB1 level difference discriminating between correct vs. incorrect implantation. Nevertheless, if we assume that the data illustrated in the lower panels of fig. 10 represent a standard outcome for a correct vs. incorrect implantation test, the use of the described differences on the resonance peak, such as the frequency shift, the level increase in the BTE PSD, and the constant level in the AB1 PSD, could indeed be combined and used in a quantitative descriptor. It must be noticed that, due to the strong intermicrophone and intersession variability shown in fig. 10, such a descriptor would, likely, be limited to a within-subject use. A possible

scenario would involve, e. g., the monitoring of an implanted patient over time: in such a case, a variation in the response over time (using a postoperative healing measurement as a reference) might indicate possible complications in the implantation.

A more quantitative and simplified description of the nonlinearities has been given by means of the distortion measure D. The data have shown that increased nonlinearities are to be expected as the stimulation level increases, possibly leading to problems when using a standard linear feedback canceller. Additionally, they have pointed out how an incorrect implantation strongly increases the value of D obtained from the BTE microphone, again making the feedback problems more severe. On the contrary, the values of D obtained from the AB1 microphone in both a correct and an incorrect implantation are comparable, suggesting that most of the additional energy from the skull vibrations does not get converted into sound radiated outside the head. The simplified description provided by the single D values, as opposed to the more dense PSDs information, combined with the seemingly (although not statistically) relevant difference of D between correctly and incorrectly implanted results from BTE and AB1 microphones, could be used to speculate the use of D as a numerical indication of an incorrect implantation. For instance, by comparing values of D measured both intra- and postoperatively, one could assess whether some postoperative complications might have occurred. Such a possibility was not investigated in the present work, but will be considered in future investigations.

D. DIFFERENCE BETWEEN TISSULAR AND AIRBORNE FEEDBACK

We mentioned that, in fig. 10, the differences between microphone signals recorded in the same session, at the same level, should be attributable to the feedback path alone. This simplification might not be met within the whole frequency spectrum in our measurements, since the noise floors of both the microphones, respectively 10 and 5 dB SPL [25] for the BTE and the AB1 microphone, are comparable with the lower recorded levels. However, above these values the comparison should hold. Additionally, various spectral portions of the measured signals were in proximity of the noise floor and this partially limits the usability of the microphone signal PSDs within those frequencies. Fortunately, this is not necessarily the case for the DIRs in fig. 9, given the good performance of the ESS technique in the presence of pink background noise, similar to the one recorded during the measurements [18], [21].

The overall trend in the results seems to confirm our hypothesis of a difference in the feedback paths defined by the two microphones and it is plausible to attribute part of the discrepancy to the presence of a tissular component in the feedback path to the BTE microphone not being picked-up by the AB1 microphone. Specifically, we believe that the direct mechanical coupling of the sound processor (and thus the BTE microphone) to the implant (through the bone and soft tissue layers) is responsible for this phenomenon. For this reason, we were initially expecting stronger peak components in the BTE microphone PSD compared to the AB1 microphone PSD, such as in the extreme case of an incorrect implantation in the lower panels of fig. 10. However, in the comparison between the two microphone signals from MS1 and MS2 in fig. 10 the opposite occurs. The higher value of the AB1 microphone PSDs could be due to the specific position of the two microphones with respect to the actuator and the tested ear. Given the proximity between the microphones and the sound radiating source, near-field effects can be expected, such as strongly directional radiation patterns possibly leading to the different levels measured by the microphones. Nevertheless, we cannot necessarily rule out the possibility of a measurement artifact. Almost no level discrepancy was shown between the BTE and AB1 microphone PSDs in MS4. This could be due to the fact that the previously mentioned effects are dependent on the specific anatomy of the specimen and, hence, not expected in each measurements. Although these are just hypotheses accounting for said difference and the true mechanism was not investigated further, low values of the BTE microphone PSDs are preferred in a real scenario, as they would limit the occurrence of acoustic feedback.

V. CONCLUSIONS

In this study, we have measured the feedback path of the Cochlear Codacs DACI on fresh frozen cadaver heads. The measurements provide four important answers to the same number of initial general objectives: 1) The difference between the signals recorded by the different microphones in the different MSs indicate that there is clearly a dependence of the measured feedback path on the implanted specimen; 2) An incorrect implantation can strongly affect the measured feedback; 3) The response of the actuator is indeed nonlinear at the measured levels and the nonlinearities characterizing such response are shaped by the specimen-dependent mechanical coupling; 4) The difference between the feedback paths from the actuator to the different microphones points out the presence of a tissular feedback component in the BTE microphone, more slowly decaying than the airborne component recorded in both microphones. Combining the outcomes of these findings, especially from 2) and 3), in a closed-loop scenario could exacerbate the different individual problems, potentially leading to acoustic feedback artifacts.

The next step of our investigation will focus on the testing of the DACI in a more realistic closed-loop scenario, to observe whether the use of some simple feedback-cancellation strategies can cope with possible feedback problems and to evaluate whether the information described in this paper can be effectively used to improve the cancellation performance of an AFC algorithm.

ACKNOWLEDGMENTS

The authors would like to thank Dr. A. T. Rosell (Technical University of Denmark, DK), Dr. J. Walraevens and A. Gozzi (Cochlear Technology Centre Belgium, BE), and

Dr. J.-M. Gérard (Saint-Luc University Hospital, BE). This paper was presented in part at the 2014 International Hearing Aid Research Conference, Lake Tahoe, CA, USA, and at the 2015 Conference on Implantable Auditory Prostheses, Lake Tahoe, CA, USA.

REFERENCES

[1] R. Häusler, C. Stieger, H. Bernhard, and M. Kompis, "A novel implantable hearing system with direct acoustic cochlear stimulation," *Audiol. Neurotol.*, vol. 13, no. 4, pp. 247–256, Nov. 2008.
[2] N. Verhaert, C. Desloovere, and J. Wouters, "Acoustic hearing implants for mixed hearing loss: A systematic review," *Otol. Neurotol.*, vol. 34, no. 7, pp. 1201–1209, Sep. 2013.
[3] T. Lenarz *et al.*, "A comparative study on speech in noise understanding with a direct acoustic cochlear implant in subjects with severe to profound mixed hearing loss," *Audiol. Neurotol.*, vol. 19, no. 3, pp. 164–174, Jul. 2014.
[4] T. Lenarz *et al.*, "Multicenter study with a direct acoustic cochlear implant," *Otol. Neurotol.*, vol. 34, no. 7, pp. 1215–1225, Sep. 2013.
[5] T. van Waterschoot and M. Moonen, "Fifty years of acoustic feedback control: State of the art and future challenges," *Proc. IEEE*, vol. 99, no. 2, pp. 288–327, Feb. 2011.
[6] J. A. Maxwell and P. M. Zurek, "Reducing acoustic feedback in hearing aids," *IEEE Trans. Speech Audio Process.*, vol. 3, no. 4, pp. 304–313, Jul. 1995.
[7] J. M. Kates, "Feedback cancellation in hearing aids: Results from a computer simulation," *IEEE Trans. Signal Process.*, vol. 39, no. 3, pp. 553–562, Mar. 1991.
[8] T. van Waterschoot, G. Rombouts, and M. Moonen, "Optimally regularized adaptive filtering algorithms for room acoustic signal enhancement," *Signal Process.*, vol. 88, no. 3, pp. 594–611, Mar. 2008.
[9] P. Estermann and A. Kaelin, "Feedback cancellation in hearing aids: Results from using frequency-domain adaptive filters," in *Proc. IEEE Int. Symp. Circuits Syst. (ISCAS)*, vol. 2. May 1994, pp. 257–260.
[10] N. Madhu, J. Wouters, A. Spriet, T. Bisitz, V. Hohmann, and M. Moonen, "Study on the applicability of instrumental measures for black-box evaluation of static feedback control in hearing aids," *J. Acoust. Soc. Amer.*, vol. 130, no. 2, pp. 933–947, Aug. 2011.
[11] J. Hellgren, T. Lunner, and S. Arlinger, "Variations in the feedback of hearing aids," *J. Acoust. Soc. Amer.*, vol. 106, no. 5, pp. 2821–2833, 1999. [Online]. Available: http://scitation.aip.org/content/asa/journal/jasa/106/5/10.1121/1.428107
[12] D. K. Bustamante, T. L. Worrall, and M. J. Williamson, "Measurement and adaptive suppression of acoustic feedback in hearing aids," in *Proc. Int. Conf. Acoust., Speech, Signal Process. (ICASSP)*, vol. 3. May 1989, pp. 2017–2020.
[13] M. G. Siqueira, R. Speece, E. Petsalis, A. Alwan, S. Soli, and S. Gao, "Subband adaptive filtering applied to acoustic feedback reduction in hearing aids," in *Proc. Conf. Rec. 13th Asilomar Conf. Signals, Syst. Comput.*, vol. 1. Nov. 1996, pp. 788–792.
[14] A. Farina, "Simultaneous measurement of impulse response and distortion with a swept-sine technique," in *Proc. AES 108th Conv.*, Paris, France, Feb. 2000, paper 5093. [Online]. Available: http://www.aes.org/e-lib/browse.cfm?elib=10211
[15] *Standard Practice for Describing System Output of Implantable Middle Ear Hearing Devices*, Standard A. S. F2504-05, 2014.
[16] H. Bernhard, C. Stieger, and Y. Perriard, "Design of a semi-implantable hearing device for direct acoustic cochlear stimulation," *IEEE Trans. Biomed. Eng.*, vol. 58, no. 2, pp. 420–428, Feb. 2011.
[17] A. Torras-Rosell and F. Jacobsen, "A new interpretation of distortion artifacts in sweep measurements," *J. Audio Eng. Soc.*, vol. 59, no. 5, pp. 283–289, Jun. 2011. [Online]. Available: http://www.aes.org/e-lib/browse.cfm?elib=15929
[18] A. Torras-Rosell, "Methods of measuring impulse responses in architectural acoustics," M.S. thesis, Dept. Electr. Eng., Tech. Univ. Denmark, Lyngby, Denmark, 2009.
[19] A. Spriet, G. Rombouts, M. Moonen, and J. Wouters, "Adaptive feedback cancellation in hearing aids," *J. Franklin Inst.*, vol. 343, no. 6, pp. 545–573, Aug. 2006.
[20] M. G. Siqueira and A. Alwan, "Steady-state analysis of continuous adaptation in acoustic feedback reduction systems for hearing-aids," *IEEE Trans. Speech Audio Process.*, vol. 8, no. 4, pp. 443–453, Jul. 2000.
[21] G.-B. Stan, J.-J. Embrechts, and D. Archambeau, "Comparison of different impulse response measurement techniques," *J. Audio Eng. Soc.*, vol. 50, no. 4, pp. 249–262, Apr. 2002. [Online]. Available: http://www.aes.org/e-lib/browse.cfm?elib=11083
[22] M. Grossöhmichen, R. Salcher, H.-H. Kreipe, T. Lenarz, and H. Maier, "The codacs direct acoustic cochlear implant actuator: Exploring alternative stimulation sites and their stimulation efficiency," *PLoS ONE*, vol. 10, no. 3, p. e0119601, 2015.
[23] D. Havelock, S. Kuwano, and M. Vorländer, *Handbook of Signal Processing in Acoustics*. New York, NY, USA: Springer, 2008.
[24] J. W. Zwartenkot, A. F. Snik, E. A. Mylanus, and J. J. Mulder, "Amplification options for patients with mixed hearing loss," *Otol. Neurotol.*, vol. 35, no. 2, pp. 221–226, 2014.
[25] Brüel & Kjær. (1995). *Microphone Handbook for the FalconTM Range of Microphone Products*. [Online]. Available: www.bksv.com/doc/ba5105.pdf



GIULIANO BERNARDI (S'12) was born in Asolo, Italy, in 1987. He received the M.Sc. degree in engineering acoustics from Denmark Technical University, Denmark, in 2011, and the M.Eng. degree in bioengineering from the University of Padua, Padua, Italy, in 2012. He is currently pursuing the Ph.D. degree with the STADIUS Research Division, Department of Electrical Engineering, Katholieke Universiteit (KU) Leuven.

His research focuses on acoustic feedback control, specifically for hearing-aid applications.



TOON VAN WATERSCHOOT (S'04–M'12) received the M.Sc. degree and the Ph.D. degree in electrical engineering from Katholieke Universiteit (KU) Leuven, Belgium, in 2001 and 2009, respectively.

He has previously held teaching and research positions with the Antwerp Maritime Academy, the Institute for the Promotion of Innovation through Science and Technology in Flanders, and the Research Foundation–Flanders, Belgium, with the Delft University of Technology, The Netherlands, and with the University of Lugano, Switzerland. He is currently a tenure-track Assistant Professor with KU Leuven. His research interests are in signal processing, machine learning, and numerical optimization, applied to acoustic signal enhancement, acoustic modeling, audio analysis, and audio reproduction.

Dr. van Waterschoot is a member of EURASIP, ASA, and AES. He is a member of the Board of Directors of the European Association for Signal Processing (EURASIP) and a member of the IEEE Audio and Acoustic Signal Processing Technical Committee. He was the General Chair of the 60th AES International Conference, Leuven, Belgium (2016), and has been serving on the Organizing Committee of the European Conference on Computational Optimization (EUCCO 2016) and the IEEE Workshop on Applications of Signal Processing to Audio and Acoustics (WASPAA 2017). He has been serving as an Associate Editor of the *Journal of the Audio Engineering Society* and the *EURASIP Journal on Audio, Music, and Speech Processing*, and as a Guest Editor of *Elsevier Signal Processing*.



MARC MOONEN (M'94–SM'06–F'07) is a Full Professor with the Electrical Engineering Department of Katholieke Universiteit (KU) Leuven, where he is heading a research team involved in the area of numerical algorithms and signal processing for digital communications, wireless communications, DSL, and audio signal processing.

He received the 1994 KU Leuven Research Council Award, the 1997 Alcatel Bell (Belgium) Award (with Piet Vandaele), the 2004 Alcatel Bell (Belgium) Award (with Raphael Cendrillon), and was a 1997 Laureate of the Belgium Royal Academy of Science. He received journal best paper awards from the IEEE TRANSACTIONS ON SIGNAL PROCESSING (with Geert Leus and with Daniele Giacobello) and from *Elsevier Signal Processing* (with Simon Doclo).

He was Chairman of the IEEE Benelux Signal Processing Chapter (1998–2002), a member of the IEEE Signal Processing Society Technical Committee on Signal Processing for Communications, and the President of EURASIP (European Association for Signal Processing, 2007–2008 and 2011–2012).

He has served as an Editor-in-Chief of the *EURASIP Journal on Applied Signal Processing* (2003–2005), an Area Editor of the Feature Articles in *IEEE Signal Processing Magazine* (2012–2014), and has been a member of the editorial board of the IEEE TRANSACTIONS ON CIRCUITS AND SYSTEMS II, *IEEE Signal Processing Magazine*, *Integration-the VLSI Journal*, *EURASIP Journal on Wireless Communications and Networking*, *EURASIP Journal on Applied Signal Processing*, and *EURASIP Signal Processing*.



JAN WOUTERS was born in 1960. He received the master's and Ph.D. degrees in physics from the University of Leuven, Katholieke Universiteit (KU) Leuven, Leuven, Belgium, in 1982 and 1989, respectively, with intermission for officer military service.

From 1989 to 1992, he was a Post-Doctoral Research Fellow with the Belgian National Fund for Scientific Research, Institute of Nuclear Physics, Catholic University of Louvain, Louvain-la-Neuve and with the NASA Goddard Space Flight Center, USA. Since 1993, he has been a Professor with the Department of Neurosciences, KU Leuven, and has been a Full Professor, since 2005. His current research interests include audiology and the auditory system, signal processing for cochlear implants, and hearing aids.

Dr. Wouters is the Editorial Board of the *International Journal of Audiology*, the *Journal of Communication Disorders*, and the *Journal B-ENT*. He is the President of the European Federation of Audiological Societies and the Belgian Audiological Society. He is a member of the International Collegium for ORL, and a Board Member of the International Collegium for Rehabilitative Audiology.



MARTIN HILLBRATT was born in 1973. He received the M.Sc. degree in electrical engineering from Chalmers Technical University, Gothenburg, Sweden, in 2004.

He has been with signal processing and especially feedback reduction algorithms within Entific (2004–2005) and Cochlear (2005–2016). He has filed numerous patents in the field of hearing devices and several related to signal processing solutions.



NICOLAS VERHAERT received the M.D. degree and the Ph.D. degree in biomedical sciences from Katholieke Universiteit (KU) Leuven, Belgium, in 2004 and 2014, respectively. After his training as a specialist in Otorhinolaryngology, Head and Neck surgery with University Hospitals Leuven and General Hospital Bruges, he graduated and was recognized by the Belgian Ministry of Health in 2009. From 2009 to 2011, he performed ENT fellowships abroad in the University Hospitals of Lyon, France, and at the Hannover Medical School, Germany, focusing on otology, hearing implants, and neuro-otology. Since 2011, he has been a Staff Surgeon with the Department of Otorhinolaryngology, Head and Neck Surgery of University Hospitals Leuven and Researcher at the research group ExpORL from the Department of Neurosciences, KU Leuven. He obtained research grants from Research Foundation Flanders (2011–2013) and Research Council of the University Hospitals Leuven (2013–2015).

He is currently involved into otology and neurotology surgery, including cochlear and middle ear implants. His translational research lies in the field of acoustic hearing implants with a focus on middle ear implants and DACI devices. His research interests are in electrophysiological measurements, fitting, signal processing in hearing implants, middle ear mechanics, and clinical otology. He obtained a grant from Research Foundation Flanders as a Senior Clinical Investigator (2015–2020).

Dr. Verhaert is Reviewer of the *International Journal of Pediatric ORL* and the *Journal B-ENT*. Since 2015, he will be teaching ENT courses at the Speech & Languages therapy and Audiology sciences at KU Leuven. He is member of European academy of Otology, Neurotology and the Belgian Society of ENT and B-Audio.